# Regular Boundary Integral Formulation for the Analysis of Open Dielectric/Optical Waveguides

Yukio Kagawa, *Fellow, IEEE*, Yonghao Sun, and Zaheed Mahmood

*Abstract*—**Regular boundary element method is employed for the variational formulation of Helmholtz equation that governs the waveguiding problems. The problems are defined on the boundary as usual, but like in the charge simulation method, the source points associated with the fundamental solutions are allocated outside the domain so that the singular integrals which occur in the standard boundary element procedure can be avoided. First, the formulation is developed for the two-dimensional (2-D) scalar Helmholtz problem solving for the axial components of either electric or magnetic fields. Then the formulation is extended for the analysis of dielectric waveguides of open type incorporating axial components of both electric and magnetic fields, for the solution of the propagating modes which are generally of hybrid types. Very close agreements have been found when the solutions obtained by the present formulation are compared with the ones obtained by different methods. One merit of the extended formulation is that it has been fixed to suppress the spurious solutions.**

## I. Introduction

DESPITE THE FACT that many things are common between the boundary element method (BEM) and the charge simulation method (CSM) [1] there exists an underlying difference in their treatment of boundary value satisfaction. In BEM, the boundary of the domain under consideration is divided into elements and the value at an arbitrary point on the boundary is expressed by the proper interpolation of the nodal values. One can then write boundary integral equation associated with the Green functions, resulting in discretized simultaneous linear equations for the nodes. In CSM, a form of linear combination of Green functions is chosen to satisfy the boundary values evaluated at discrete points for the simulated charges arranged outside the domain, along the boundary. One drawback of the BEM is that the kernel of the boundary integral consists of a singular function often difficult to integrate. Under this circumstances, Patterson and Sheikh proposed a regular boundary element method which is the same as the conventional BEM except that the singularity associated with the fundamental solutions is eliminated by shifting the source terms outside the domain as in CSM, obtaining a system of regular boundary integrals. Patterson applied this approach successfully to fluid and elastic problems [2]. Honma also solved convective diffusion problems [3] using the same approach.

The errors of solutions obtained by conventional and regular BEM are known to be pronounced in the vicinity of the boundary, while the same for CSM depend on the locations chosen for the simulated charges. It is therefore necessary to arrange the simulated charges appropriately for obtaining accurate solutions. Taking proper consideration of these things, we have proposed variational boundary element formulations and applied them to the Laplace and Helmholtz problems [4]–[5]. Then in order to avoid singular integrals, we also have developed [6] the variational formulation of regular boundary integrals for the Laplace problems. Here in this paper, we apply the same approach of regular boundary element method based on variational principle to Helmholtz problems.

First, the variational formulation of regular boundary integral is developed for waveguide analysis governed by Helmholtz equation. The formulation is applied to a simple hollow rectangular waveguide and dielectric slab and ridge loaded waveguide, solving for the wave number of the propagating modes which are of transverse type. Then the formulation is shown to be extended for the application to unbounded problems of a dielectric/optical waveguide. As the dielectric waveguides are of open type, the exterior domain is considered to be extended to infinity. The BEM provides advantages right at this point, because it can easily be applied to open-type problems. Sano and Kurazono [7] also used BEM for the open-type eigenvalue problems. For the application to open-type dielectric waveguiding problems, the extensions made in the formulations are:

1) As the propagating modes are hybrid, the variational formulation incorporates the axial components of both electric and magnetic fields which are coupled by the continuity conditions of the electromagnetic fields at the interface between dielectrics;
2) The formulation is modified to yield spurious-free solutions by incorporating explicitly the continuity of the tangential derivatives of the fields.

Only the drawback of the present formulation is that as the wave number to be resolved spreads out in the discretized equation in a scattered manner, it must be solved by determinant search technique.

## II. Variational Boundary Element Formulation

The two-dimensional (2-D) Helmholtz equation representing a wave equation and the associated boundary conditions are given by

$$\nabla^2\phi + k^2\phi = 0 \quad \text{in } \Omega$$
$$\phi = \hat{\phi} \quad \text{in } \Gamma_1$$

Manuscript received December 1, 1995; revised April 19, 1996.

The authors are with the Department of Electrical and Electronic Engineering, Okayama University, Okayama 700, Japan.

Publisher Item Identifier S 0018-9480(96)05651-7.

$$\frac{\partial \phi}{\partial \boldsymbol{n}} = \hat{q} \quad \text{in } \Gamma_2 \tag{1}$$

where $k$ is the wave number, $\boldsymbol{n}$ is a unit normal vector pointing outward at the boundary, $\Gamma = \Gamma_1 + \Gamma_2$ denotes the boundary of the domain $\Omega$, $\hat{\phi}$ is the potential and $\hat{q}$ is the flux of known quantities prescribed over the boundaries $\Gamma_1$ and $\Gamma_2$, respectively. The energy functional corresponding to (1) is given by

$$\Pi(\phi) = \tfrac{1}{2}\int_{\Omega}\{(\nabla\phi)^2 - k^2\phi^2\}\, d\Omega - \int_{\Gamma_2}\phi\hat{q}\, d\Gamma. \tag{2}$$

Based on the hybrid method of P.Tong and Rossettos [8], on defining $\tilde{\phi}$ and $\tilde{q}$ generally over the boundary $\Gamma$, (2) leads to the hybrid functional

$$\Pi(\phi,\tilde{\phi},\tilde{q}) = \tfrac{1}{2}\int_{\Omega}\{(\nabla\phi)^2 - k^2\phi^2\}\, d\Omega - \int_{\Gamma}(\phi-\tilde{\phi})\tilde{q}\, d\Gamma - \int_{\Gamma_2}\tilde{\phi}\hat{q}\, d\Gamma. \tag{3}$$

Applying variational principle to (3) and making the functional stationary with respect to $\phi, \tilde{\phi}$ and $\tilde{q}$, the governing equation

$$\nabla^2\phi + k^2\phi = 0 \quad \text{in } \Omega$$

and the boundary conditions

$$\begin{aligned} \phi &= \tilde{\phi} \quad \text{on } \Gamma \\ \tilde{\phi} &= \hat{\phi} \quad \text{on } \Gamma_1 \\ q &= \tilde{q} \quad \text{on } \Gamma \\ \tilde{q} &= \hat{q} \quad \text{on } \Gamma_2 \end{aligned}$$

are obtained for the Helmholtz problem. After carrying out integration on (3) by parts, the domain integral is eliminated leaving a functional which consists of boundary integrals only

$$\Pi(\phi,\tilde{\phi},q,\tilde{q}) = \tfrac{1}{2}\int_{\Gamma}\phi q\, d\Gamma - \int_{\Gamma}(\phi-\tilde{\phi})\tilde{q}\, d\Gamma - \int_{\Gamma_2}\tilde{\phi}\hat{q}\, d\Gamma. \tag{4}$$

At this point, the discretized formulation for the boundary element method is considered. Locating simulated charges $\alpha_j (j = 1, 2, \cdots, L)$ outside the domain, the potential at any arbitrary point $i$ in the field is expressed in terms of the linear combination of the contribution from each source $\alpha_j$ as

$$\phi_i = \sum_{j=1}^{L}\phi^*_{ji}\alpha_j = \{\phi^*\}_i^T\{\alpha\} \tag{5}$$

where

$$\{\phi^*\}_i = \{\phi^*_{1i}\phi^*_{2i}\cdots\phi^*_{Li}\}, \quad \{\alpha\} = \{\alpha_1\alpha_2\cdots\alpha_L\}$$

$\phi_{ji}$ is the fundamental solution whose value is evaluated at point $i$ for a unit source given at point $j$ outside the domain, and $\alpha_j$ is the unknown coefficient associated with the simulated charge source at location $j$. The boundary is divided into elements $\Gamma_m (m = 1, 2, \cdots, M)$. The potential at the point $i$ within the element $m$ is expressed in terms of the interpolation between the nodal values as

$$\tilde{\phi}_i = \{N_{\tilde{\phi}}\}^T\{\tilde{\phi}\}_m \quad \text{and} \quad \tilde{q}_i = \{N_{\tilde{q}}\}^T\{\tilde{q}\}_m \tag{6}$$

where

$$\{\tilde{\phi}\}_m = \{\tilde{\phi}_{m1}\tilde{\phi}_{m2}\}, \quad \{\tilde{q}\}_m = \{\tilde{q}_{m1}\tilde{q}_{m2}\}$$

are the potential and the flux vector defined at the terminals of the element, that is, at the nodes. The elements considered here are constant elements for which all the components of the interpolation vector $\{N_{\tilde{\phi}}\}$ and $\{N_{\tilde{q}}\}$ become 1/2, since at any point of an element, the values of $\tilde{\phi}_i$ and $\tilde{q}_i$ are taken to be the average of the terminal values of the element.

The fundamental solution for the Helmholtz equation and its normal derivative are given [9] by

$$\phi^*_{ji} = \frac{1}{4\sqrt{-1}}H_0^{(2)}(kR_{ji}) \quad \text{and}$$
$$\frac{\partial\phi^*_{ji}}{\partial\boldsymbol{n}} = -\frac{\boldsymbol{n}_x X + \boldsymbol{n}_y Y}{4\sqrt{-1}R_{ji}}kH_1^{(2)}(kR_{ji})$$

where $R_{ji} = \sqrt{[X^2+Y^2]}, X = x_j - x_i, Y = y_j - y_i, H_0^{(2)}$ and $H_1^{(2)}$ are, respectively, the zeroth and first order Hankel function of second kind, and $\boldsymbol{n}_x$ and $\boldsymbol{n}_y$ are, respectively, the directed cosines, the x and y directed components of the outward unit normal $\boldsymbol{n}$. Substitution of (5) and (6) in (4) leads to

$$\begin{aligned}\Pi(\alpha,\tilde{\phi},\tilde{q}) &= \sum_{i=1}^{M}\left\{\frac{1}{2}\int_{\Gamma_i}\phi_i\frac{\partial\phi_i}{\partial\boldsymbol{n}}\, d\Gamma_i - \int_{\Gamma_i}(\phi_i-\tilde{\phi}_i)\tilde{q}_i\, d\Gamma_i - \int_{\Gamma_{2i}}\tilde{\phi}_i\hat{q}_i\, d\Gamma_{2i}\right\} \\ &= \frac{1}{2}\{\alpha\}^T[H]\{\alpha\} - \{\alpha\}^T[G]\{\tilde{q}\} + \{\tilde{\phi}\}^T[L]\{\tilde{q}\} - \{\tilde{\phi}\}^T[P]\{\hat{q}\}\end{aligned} \tag{7}$$

where

$$\{\tilde{\phi}\} = \{\tilde{\phi}_1\tilde{\phi}_2\cdots\tilde{\phi}_M\}, \quad \{\tilde{q}\} = \{\tilde{q}_1\tilde{q}_2\cdots\tilde{q}_M\} \quad \text{and}$$
$$\{\hat{q}\} = \{\hat{q}_1\hat{q}_2\cdots\hat{q}_N\}, \qquad (N \le M)$$

and the components of the matrices $[H]$ and $[G]$ are given by

$$H_{jk} = \sum_{m=1}^{M}\int_{\Gamma_m}\phi^*_{jm}\frac{\partial\phi^*_{km}}{\partial\boldsymbol{n}}\, d\Gamma_m,$$
$$G_{jm} = \int_{\Gamma_m}\phi^*_{jm}\, d\Gamma_m \qquad (j,k = 1,2,\cdots,L, m = 1,2,\cdots,M).$$

In (7), $[L]$ and $[N]$ are diagonal matrices, where the component of $[L]$ corresponds to the length of each element of the boundary $\Gamma$ and that of $[N]$ correspond to the length of each element of the boundary $\Gamma_2$.

After applying variational principle to (7) by making the functional stationary with respect to $\alpha$ and $\tilde{q}$, we obtain

$$\delta\Pi_\alpha = [F]\{\alpha\} - [G]\{\tilde{q}\} = 0 \tag{8}$$
$$\delta\Pi_{\tilde{q}} = [L]\{\tilde{\phi}\} - [G]^T\{\alpha\} = \{0\}. \tag{9}$$

The equation obtained by eliminating $\alpha$ from (8) and (9) is given by

$$[K]\{\tilde{\phi}\} - [G]\{\tilde{q}\} = \{0\} \tag{10}$$

where $[K] = [F][R]$ with $[R] = ([G]^{-1})^T[L]$ and

$$F_{jk} = \frac{1}{2}\sum_{m=1}^{M}\int_{\Gamma_m}\phi^*_{jm}\frac{\partial\phi^*_{km}}{\partial \boldsymbol{n}}\,d\Gamma_m + \frac{1}{2}\sum_{m=1}^{M}\int_{\Gamma_m}\phi^*_{km}\frac{\partial\phi^*_{jm}}{\partial \boldsymbol{n}}\,d\Gamma_m.$$

For the 2-D Helmholtz problem, (10) represent the regular boundary element formulation based on variational principle. Note that as the simulated charges are arranged outside the domain, the kernels involved with (10) do not contain any singular expressions so that the integrals can readily be evaluated.

### A. Application to Hollow Waveguides

The application of the regular boundary element formulation of the previous section is made to the modal analysis of hollow waveguiding problem. It is an eigenvalue problem of free vibration type. The eigenvalue formulation correspond to TE and TM mode analysis in accordance with the applied boundary conditions of $\{\hat{q}\} = 0$ and $\{\hat{\phi}\} = 0$, respectively.

For TE mode, (10) becomes

$$[K(k)]\{\tilde{\phi}\} = \{0\}. \tag{11}$$

Here the complex functions $[K(k)]$ and $\{\tilde{\phi}\}$ are divided into their real and imaginary part as

$$[K(k)] = [K_R] + [K_I] \quad \text{and} \quad \{\tilde{\phi}\} = \{\tilde{\phi}_R\} + \{\tilde{\phi}_I\}$$

so that (11) can be written [10] as

$$\begin{bmatrix}[K_R] & [K_I]\\ [K_I] & [K_R]\end{bmatrix}\begin{bmatrix}\{\tilde{\phi}_R\}\\ \{\tilde{\phi}_I\}\end{bmatrix} = \{0\}. \tag{12}$$

The eigenvalues $k$ are are the roots of the determinant

$$\det\begin{vmatrix}[K_R] & [K_I]\\ [K_I] & [K_R]\end{vmatrix} = 0. \tag{13}$$

Again, considering only the real part of the equations corresponding to eigenvalue $k$, we have

$$\det|[K_R]| = 0. \tag{14}$$

For TM mode, (10) becomes

$$[G]\{\tilde{q}\} = \{0\}. \tag{15}$$

As $[G]$ and $\{\tilde{q}\}$ are again complex, the roots or the eigenvalues are obtained by the same way as described for TE modes.

At this point, a rectangular hollow waveguide is studied and the eigenvalue solutions for the TM and TE modes are compared with the theoretical ones. The matrices $[K]$ and $[G]$ become complex quantities as they comprise integrals associated with hankel functions and exponential functions. As the resolving parameter $k$ spreads out in the formulation in a scattered manner, the formulation can no longer be solved by standard eigenvalue solver. Under this circumstances, (11) and (15) are solved by determinant search technique where the numerical computations are carried out by putting different values of $k$ for a certain span of interest. The values of $k$ are taken to be its solutions at which the determinant of the system matrix becomes zero. Thus, (13) and (14) are solved for $k$ and detailed searching is carried out at the regions where the values of both the determinants approach zero. Fig. 1 shows a rectangular Helmholtz field where the rectangular boundary is shown to be divided into 24 constant elements and the same number of the simulated charges are shown to be allocated outside the domain along the boundary. The determinant values are plotted in Figs. 2 and 3 for TE and TM modes, respectively, for different values of $k$. The results are compared in Table I with the theoretical ones and the ones obtained by dual reciprocity method (DRM). One of the entries of the DRM column is shown vacant as the solution obtained is far away from the theoretical one.

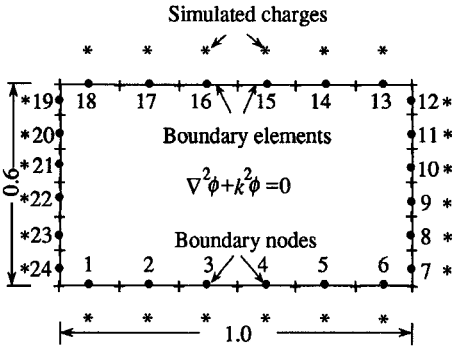


Fig. 1. Rectangular Helmholtz field with boundary elements, nodes, and simulated charges.

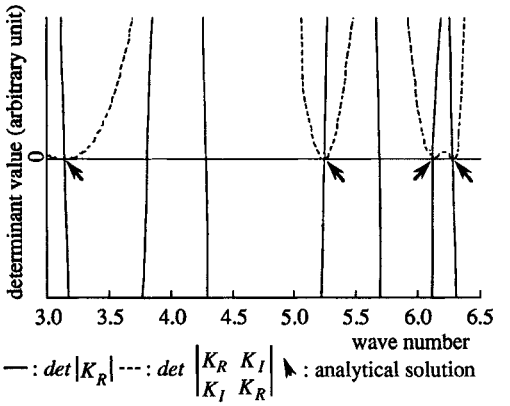


Fig. 2. Variation of determinant value for wave number.

Next, the eigenvalue solutions of a hollow rectangular waveguide [11] with mixed boundary conditions are obtained by applying the present formulation. The mixed boundary conditions are

$$\begin{aligned}\phi = \hat{\phi} = 0 \quad &\text{on } \Gamma_1\\ \frac{\partial\phi}{\partial \boldsymbol{n}} = \hat{q} = 0 \quad &\text{on } \Gamma_2.\end{aligned} \tag{16}$$

Substitution of (16) into (10) leads to

$$[[K_1] \quad [K_2]]\begin{bmatrix}\{0\}\\ \{\phi_2\}\end{bmatrix} = [[G_1] \quad [G_2]]\begin{bmatrix}\{q_1\}\\ \{0\}\end{bmatrix}. \tag{17}$$

Here the subscripts 1 and 2 represent the components corresponding to the boundaries $\Gamma_1$ and $\Gamma_2$, respectively, where

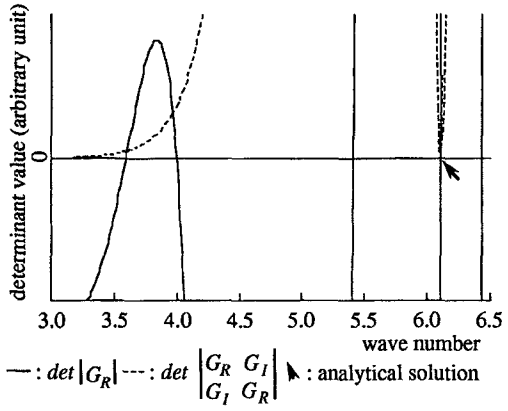


Fig. 3. Variation of determinant value for wave number.

TABLE I
ANALYTICAL AND NUMERICAL SOLUTIONS OF SOME LOWER MODE

| Mode | Exact | Present Method | DRM |
|---|---|---|---|
| $TE_{10}$ | 3.14 | 3.14 | 3.19 |
| $TE_{01}$ | 5.23 | 5.23 | 5.52 |
| $TE_{11}$ | 6.10 | 6.10 | 6.24 |
| $TE_{20}$ | 6.28 | 6.28 | 6.71 |
| $TM_{11}$ | 6.10 | 6.10 | – |

DRM : Calculated by Dual Reciprocity Method

known quantities of potential and flux are prescribed. Rearranging (17), we obtain

$$[[-G_1] \quad [K_2]]\begin{bmatrix}\{q_1\}\\ \{\phi_2\}\end{bmatrix} = [[-K_1] \quad [G_2]]\begin{bmatrix}\{0\}\\ \{0\}\end{bmatrix} \tag{18}$$

which is of the form

$$[A]\{x\} = [C]\{0\} \tag{19}$$

(19) represents the eigenvalue problem defined by simultaneous (10), where the boundary conditions are given by (16). The condition for the nontrivial solution is given by

$$\det|[A]| = 0. \tag{20}$$

Fig. 4 shows rectangular Helmholtz field in which the mixed boundary conditions are shown to be prescribed on different parts of the rectangular boundary. The boundary is divided into 16 constant elements and the same number of the simulated charges are allocated outside the domain along the boundary. The variation of the determinant value with respect to the wave number is shown in Fig. 5. The eigenvalues or the wave numbers for different modes are furnished in Table II.

## III. Dielectric Loaded Waveguides

### A. Formulation

An arbitrarily shaped metal walled waveguide is considered which is composed of two homogeneous regions of different

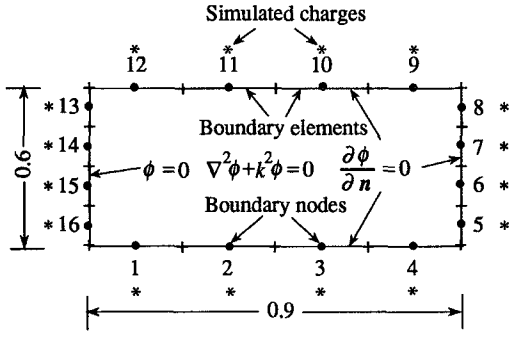


Fig. 4. Rectangular Helmholtz field with mixed boundary conditions and element division.

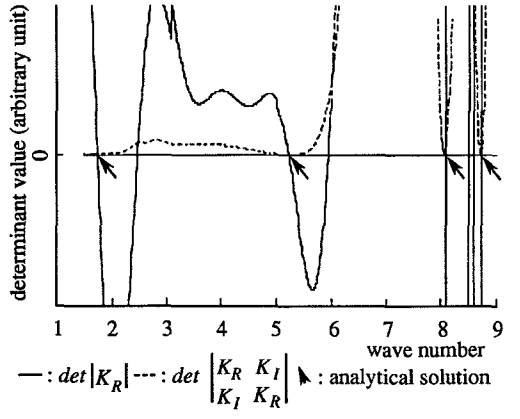


Fig. 5. Variation of determinant value for wave number.

TABLE II
ANALYTICAL AND NUMERICAL SOLUTIONS OF SOME LOWER MODE

| Mode | Exact | Present method | DRM | DRM [12] |
|---|---|---|---|---|
| $TE_{10}$ | 1.74 | 1.74 | 1.75 | 1.74 |
| $TE_{20}$ | 5.23 | 5.23 | 5.39 | 5.24 |
| $TE_{01}$ | 8.04 | 8.04 | 8.49 | – |
| $TE_{20}$ | 8.72 | 8.72 | 9.74 | 8.80 |

DRM : Calculated by Dual Reciprocity Method
DRM [12] : Results given by Partridge, Brebbia

permittivities and is uniform along the axial direction. The boundary element divisions for the different dielectric regions are carried out independently. The formulation entails proper considerations in the treatment of the coupling conditions along the interface between the two dielectrics. Along the boundary, the continuity conditions for the tangential components of the electric field $\boldsymbol{E}$ and magnetic field $\boldsymbol{H}$ are given by

$$E_{t1} = E_{t2} \quad \text{and} \quad H_{t1} = H_{t2}.$$

Considering the propagation along the axial ($z$) direction, the 2-D Helmholtz equation is given by

$$\nabla^2\phi + k^2\phi = 0 \quad \text{in } \Omega \tag{21}$$

where

$$k^2 = k_i^2 - \beta^2, \quad k_i = \omega\sqrt{\varepsilon_i \mu_i}, \quad k_0 = \omega\sqrt{\varepsilon_0 \mu_0}$$

$\omega$ is the angular frequency, $\beta$ is the propagation constant and $k$ is the wave number corresponding to materials that constitute different parts of the inhomogeneous waveguide structure. Here $\varepsilon$ and $\mu$ represent, respectively, the permittivity and permeability of the medium, and the subscript $i$ and 0 correspond to the medium $i$ and free-space, respectively. The material properties are defined as $\varepsilon_i = \varepsilon_{ri}\varepsilon_0$ and $\mu_i = \mu_{ri}\mu_0$, where $\varepsilon_r$ and $\mu_r$ are, respectively, the relative permittivity and permeability of the medium.

For the dielectric slab loaded waveguide structure of Fig. 6 which comprises two different material regions, the discretized boundary element formulation is given by

$$[[K_1] \quad [K_{1I}]]\begin{bmatrix}\{\tilde{\phi}_1\}\\ \{\tilde{\phi}_{1I}\}\end{bmatrix} - [[G_1] \quad [G_{1I}]]\begin{bmatrix}\{\tilde{q}_1\}\\ \{\tilde{q}_{1I}\}\end{bmatrix} = \{0\} \tag{22}$$

$$[[K_2] \quad [K_{2I}]]\begin{bmatrix}\{\tilde{\phi}_2\}\\ \{\tilde{\phi}_{2I}\}\end{bmatrix} - [[G_2] \quad [G_{2I}]]\begin{bmatrix}\{\tilde{q}_2\}\\ \{\tilde{q}_{2I}\}\end{bmatrix} = \{0\}. \tag{23}$$

Here the subscripts 1 and 2 correspond to the components contributed from medium 1 and 2, respectively, while the subscript $I$ correspond to the components contributed form the interface boundary between the two dielectrics. In the formulation for the TE mode (boundary condition: $\{\hat{q}\} = \{0\}$), the necessary continuity conditions required for the coupling along the interface boundary are given by

$$\tilde{\phi}_{1I} = \tilde{\phi}_{2I} = \tilde{\phi}_I, \quad (H_{z1} = H_{z2})$$
$$\tilde{q}_{1I} = \gamma\tilde{q}_{2I} = \tilde{q}_I, \quad (E_{y1} = E_{y2})$$

where

$$\gamma = -\frac{\mu_2(k_0^2\varepsilon_{r1} - \beta^2)}{\mu_1(k_0^2\varepsilon_{r2} - \beta^2)}.$$

The above conditions are used to couple the (22) and (23). After some rearrangement, the combined equation is given by

$$\begin{bmatrix}[K_1] & [K_{1I}] & [-G_{1I}] & [0]\\ [0] & [K_{21}] & [\gamma G_{2I}] & [K_2]\end{bmatrix}\begin{bmatrix}\{\tilde{\phi}_1\}\\ \{\tilde{\phi}_I\}\\ \{\tilde{q}_I\}\\ \{\tilde{\phi}_2\}\end{bmatrix} - \begin{bmatrix}[G_1] & [0]\\ [0] & [G_2]\end{bmatrix}\begin{bmatrix}\{\tilde{q}_1\}\\ \{\tilde{q}_2\}\end{bmatrix} = \{0\}. \tag{24}$$

Considering the boundary conditions, $k$ becomes the roots of the determinant

$$\det\left|\begin{bmatrix}[K_1] & [K_{1I}] & [-G_{1I}] & [0]\\ [0] & [K_{2I}] & [\gamma G_{2I}] & [K_2]\end{bmatrix}\right| = 0. \tag{25}$$

Again, the coupling conditions along the interface boundary for TM mode (boundary conditions: $\{\hat{\phi}\} = \{0\}$) are

$$\tilde{\phi}_{1I} = \tilde{\phi}_{2I} = \tilde{\phi}_I, \quad (E_{z1} = E_{z2})$$
$$\tilde{q}_{1I} = \eta\tilde{q}_{2I} = \tilde{q}_I, (H_{y1} = H_{y2})$$

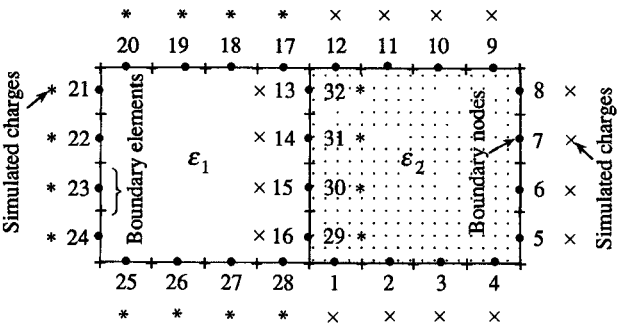


Fig. 6. Dielectric loaded waveguide: boundary elements, nodes and simulated charges.

where

$$\eta = -\frac{\varepsilon_{r2}(k_0^2\varepsilon_{r1} - \beta^2)}{\varepsilon_{r1}(k_0^2\varepsilon_{r2} - \beta^2)}$$

(22) and (23) are again combined by the above coupling conditions to yield after some rearrangement

$$\begin{bmatrix}[K_1] & [0]\\ [0] & [K_2]\end{bmatrix}\begin{bmatrix}\{\tilde{\phi}_1\}\\ \{\tilde{\phi}_2\}\end{bmatrix} - \begin{bmatrix}[G_1] & [0] & [-K_{1I}] & [G_{1I}]\\ [0] & [G_2] & [-K_{2I}] & [\eta G_{2I}]\end{bmatrix}\begin{bmatrix}\{\tilde{q}_1\}\\ \{\tilde{q}_2\}\\ \{\tilde{\phi}_I\}\\ \{\tilde{q}_I\}\end{bmatrix} = \{0\}. \tag{26}$$

The eigenvalues $k$ are obtained as the roots of the determinant

$$\det\left|\begin{bmatrix}[G_1] & [0] & [-K_{1I}] & [G_{1I}]\\ [0] & [G_2] & [-K_{2I}] & [\eta G_{2I}]\end{bmatrix}\right| = 0. \tag{27}$$

### *B. Application to Dielectric Slab Loaded Waveguides*

Fig. 6 shows the cross-sectional structure of the dielectric loaded waveguide investigated as a numerical example. Half of the waveguide is filled with dielectric material whose permittivity and permeability are equal to 2.25 and 1, respectively. The other half of the waveguide is assumed to be vacuum. The figure also shows the division of the boundary into 32 constant elements with the same number of simulated charges allocated outside the domain along the boundary. The formulation described in the previous section is solved for the eigenvalues by determinant search technique. By applying the boundary conditions for TE mode ($\{\hat{q}\} = 0$), dispersion characteristics are obtained for the dominant and a couple of higher modes, which are compared in Fig. 7 with the exact ones [13]. Fig. 8 shows the dispersion characteristic for the mode obtained by applying the boundary conditions for TM mode ($\{\hat{\phi}\} = 0$).

The next example taken for the demonstration is the dielectric ridge waveguide of Fig. 9. The eigenvalue solutions of the wave numbers are obtained for different values of permittivity of the medium with $\mu = \mu_0 = 1.0$. The solutions are compared in Table III with the analytical ones [14] and the ones obtained by the TLM method [15], where it is evident that the present formulation exhibits better accuracy.

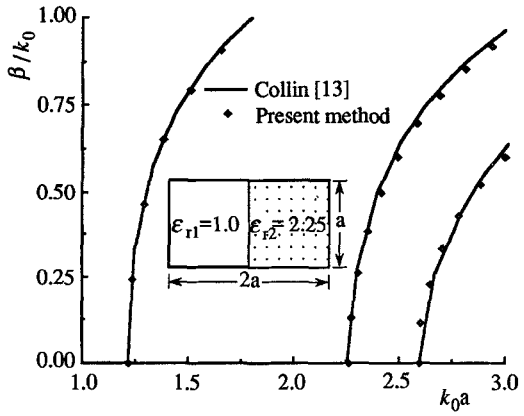


Fig. 7. Dispersion characteristics for a dielectric loaded waveguide (TE mode).

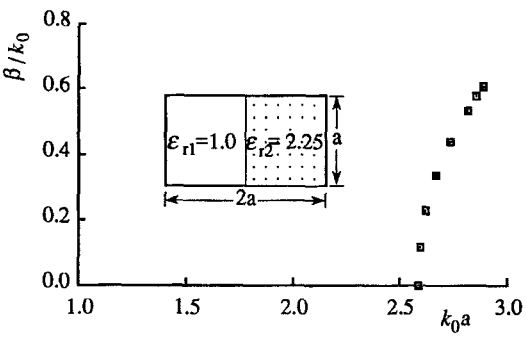


Fig. 8. Dispersion characteristic for a dielectric loaded waveguide (TM mode).

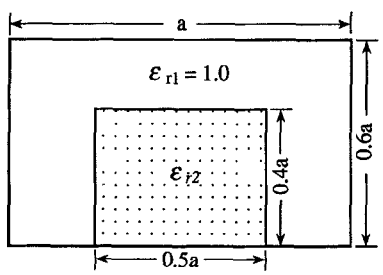


Fig. 9. Dielectric ridge waveguide.

TABLE III
CUTOFF OF DOMINANT MODE IN DIELECTRIC RIDGE WAVEGUIDE

| $\varepsilon_{r2}$ | Analytic [14] $k_0a$ | John's TLM [15] $k_0a$ | Present $k_0a$ |
|---|---|---|---|
| 2 | 2.606 | 2.62 | 2.605 |
| 3 | 2.352 | 2.36 | 2.355 |
| 4 | 2.204 | 2.22 | 2.215 |
| 6 | 2.024 | 2.04 | 2.045 |
| 8 | 1.936 | 1.96 | 1.955 |

## IV. OPEN TYPE DIELECTRIC/OPTICAL WAVEGUIDE

### A. Formulation

Considering an arbitrarily shaped inhomogeneous dielectric waveguide, the governing equation for the longitudinal

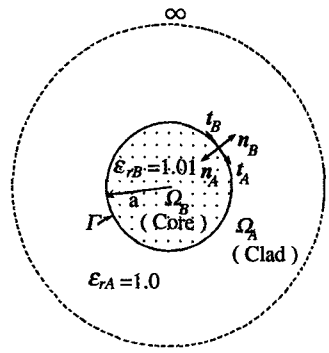


Fig. 10. Step-index fiber.

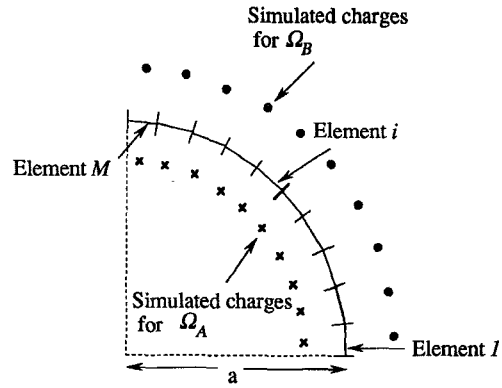


Fig. 11. Element division and simulated charge allocation for one quarter of a circular step-index fiber.

fields $(E_z, H_z)$ of the guided propagating wave along the $z$ direction is given by the same Helmholtz equation of (21), except that the equations for both fields are now considered simultaneously as

$$\nabla^2 E_z + (k_i^2 - \beta^2)E_z = 0$$
$$\nabla^2 H_z + (k_i^2 - \beta^2)H_z = 0. \tag{28}$$

Fig. 10 shows the structure of an axially symmetrical optical waveguide where the region $\Omega_A$ constitutes the clad part, and the region $\Omega_B$, the core part of the waveguide. As shown in Fig. 11, the element divisions for the different dielectric regions are carried out independently allocating the simulated charges separately for both interior and exterior regions. By applying regular BEM based on variational principle, the discretized equations are obtained as follows:

$$[K^A]\{E_z^A\} - [G^A]\left\{\frac{\partial E_z^A}{\partial n}\right\} = 0$$
$$[K^A]\{H_z^A\} - [G^A]\left\{\frac{\partial H_z^A}{\partial n}\right\} = 0 \tag{29}$$
$$[K^B]\{E_z^B\} - [G^B]\left\{\frac{\partial E_z^B}{\partial n}\right\} = 0$$
$$[K^B]\{H_z^B\} - [G^B]\left\{\frac{\partial H_z^B}{\partial n}\right\} = 0 \tag{30}$$

where

$$[K^i] = [F^i][R^i] \qquad i = A, B.$$

In the above equations, the matrices are given by the ones described in Section II, only that, the superscripts $A$ and $B$ correspond, respectively, to the regions $\Omega_A$ and $\Omega_B$, from which the matrices are contributed. The need for the combination of $E_z$ and $H_z$ in the governing equation is due to the fact that the mode propagating through a dielectric waveguide is of hybrid type, having both $E_z$ and $H_z$. The final equation is derived from the combination of the discretized (29) and (30) on application of the proper boundary conditions along the interface boundary. The tangential components of the electric and the magnetic fields should be continuous across the interface yielding

$$E_z^B = E_z^A, \quad H_z^B = H_z^A, \quad E_t^B = -E_t^A, \quad H_t^B = -H_t^A \tag{31}$$

where $E_t$ and $H_t$ are the transverse components of electric and magnetic fields, respectively, which are tangential to the boundary. The tangential components of the electromagnetic fields are given in terms of the normal and tangential derivatives of the axial components as

$$\begin{aligned} E_t^i &= \frac{j\omega\mu_i}{k_i^2-\beta^2}\left(\frac{\partial H_z}{\partial \boldsymbol{n}} - \frac{\beta}{\omega\mu_i}\frac{\partial E_z}{\partial \boldsymbol{t}}\right) \\ H_t^i &= \frac{-j\omega\varepsilon_0\varepsilon_{ri}}{k_i^2-\beta^2}\left(\frac{\partial E_z}{\partial \boldsymbol{n}} + \frac{\beta}{\omega\varepsilon_0\varepsilon_{ri}}\frac{\partial H_z}{\partial \boldsymbol{t}}\right). \end{aligned} \tag{32}$$

Inserting (32) into (31), we obtain

$$\begin{aligned} \frac{\partial H_z^B}{\partial \boldsymbol{n}} &= -\frac{\mu_A(k_B^2-\beta^2)}{\mu_B(k_A^2-\beta^2)}\frac{\partial H_z^A}{\partial \boldsymbol{n}} \\ &\quad - \frac{\beta}{\omega\mu_B}\left(1.0 - \frac{k_B^2-\beta^2}{k_A^2-\beta^2}\right)\frac{\partial E_z^A}{\partial \boldsymbol{t}} \\ \frac{\partial E_z^B}{\partial \boldsymbol{n}} &= -\frac{\varepsilon_{rA}(k_B^2-\beta^2)}{\varepsilon_{rB}(k_A^2-\beta^2)}\frac{\partial E_z^A}{\partial \boldsymbol{n}} \\ &\quad + \frac{\beta}{\omega\varepsilon_0\varepsilon_{rB}}\left(1.0 - \frac{k_B^2-\beta^2}{k_A^2-\beta^2}\right)\frac{\partial H_z^A}{\partial \boldsymbol{t}}. \end{aligned} \tag{33}$$

Thus the discretized equation obtained for (30) is

$$\begin{aligned} &[K^B]\{E_z^A\} + \frac{\varepsilon_{rA}(k_B^2-\beta^2)}{\varepsilon_{rB}(k_A^2-\beta^2)}[G^B]\left\{\frac{\partial E_z^A}{\partial \boldsymbol{n}}\right\} \\ &\quad = \frac{Z_0}{\varepsilon_{rB}}[C^B]\{H_z^A\} \\ &[K^B]\{H_z^A\} + \frac{\mu_A(k_B^2-\beta^2)}{\mu_B(k_A^2-\beta^2)}[G^B]\left\{\frac{\partial H_z^A}{\partial \boldsymbol{n}}\right\} \\ &\quad = \frac{-1}{Z_0}[C^B]\{E_z^A\}. \end{aligned} \tag{34}$$

where the component of matrix $[C^B]$ is given by

$$C_{ij}^B = \frac{\beta}{k_0}\left(1.0 - \frac{k_B^2-\beta^2}{k_A^2-\beta^2}\right)\int_{\Gamma_j}\phi_{ij}^*\frac{\partial\phi}{\partial \boldsymbol{t}}\,d\Gamma_j.$$

Here $\partial\phi/\partial \boldsymbol{t}$ represents $\partial E_z^A/\partial \boldsymbol{t}$ or $\partial H_z^A/\partial \boldsymbol{t}$. $Z_0$ is the intrinsic impedance of the free space. Combining (34) and (29), the following matrix equation is derived:

$$\begin{bmatrix} [K^A] & -[G^A] & [0] & [0] \\ [K^B] & \alpha_1[G^B] & -\dfrac{Z_0}{\varepsilon_{rB}}[C^B] & [0] \\ [0] & [0] & [K^A] & -[G^A] \\ \dfrac{1}{Z_0}[C^B] & [0] & [K^B] & \alpha_2[G^B] \end{bmatrix} \begin{bmatrix} \{E_z^A\} \\ \left\{\dfrac{\partial E_z^A}{\partial \boldsymbol{n}}\right\} \\ \{H_z^A\} \\ \left\{\dfrac{\partial H_z^A}{\partial \boldsymbol{n}}\right\} \end{bmatrix} = \begin{bmatrix} \{0\} \\ \{0\} \\ \{0\} \\ \{0\} \end{bmatrix} \tag{35}$$

where

$$\alpha_1 = \frac{\varepsilon_{rA}(k_B^2-\beta^2)}{\varepsilon_{rB}(k_A^2-\beta^2)}, \quad \alpha_2 = \frac{\mu_A(k_B^2-\beta^2)}{\mu_B(k_A^2-\beta^2)}.$$

Since $k$ enters in (35) in a scattered manner, it can no longer be solved by the standard eigenvalue solver but again by the determinant search technique.

When the example of the optical waveguide (circular step-index fiber) of Fig. 10 is solved by using (35), spurious solutions are encountered along with the physical ones. This also happens when solved by conventional BEM. As explained by Sano [7], the reason behind the occurrence of these spurious modes is the lack of continuity of tangential derivatives of the axial fields. Sano has shown that incorporation of the continuity of the tangential derivative of the fields does suppress the spurious modes. As suggested by Sano, we used $\partial E_z/\partial \boldsymbol{t}$ and $\partial H_z/\partial \boldsymbol{t}$ as the unknowns instead of $E_z$ and $H_z$ in the original formulation and as expected, we have also found the solutions completely free of the spurious ones. $\partial E_z/\partial \boldsymbol{t}$ and $\partial H_z/\partial \boldsymbol{t}$ are given by

$$\begin{aligned} E_z(\tau) &= \int_0^\tau \frac{\partial E_z}{\partial \boldsymbol{t}}\,dt + E_z(0) \\ H_z(\tau) &= \int_0^\tau \frac{\partial H_z}{\partial \boldsymbol{t}}\,dt + H_z(0) \end{aligned} \tag{36}$$

where $E_z(0)$ and $H_z(0)$ are the values of $E_z$ and $H_z$, respectively, at the reference point taken on the boundary along the integration path, and the integral is made from the reference point to the point $\tau$. For a round path of integration forming a closed loop

$$\oint_\Gamma \frac{\partial E_z}{\partial \boldsymbol{t}}\,dt = 0, \quad \oint_\Gamma \frac{\partial E_z}{\partial \boldsymbol{t}}\,dt = 0. \tag{37}$$

The new unknowns introduced are

$$\begin{aligned} \{\phi_e\} &= \left[E_z^A(0)\frac{\partial E_1^A}{\partial \boldsymbol{t}_1}\frac{\partial E_2^A}{\partial \boldsymbol{t}_2}\cdots\frac{\partial E_{M-1}^A}{\partial \boldsymbol{t}_{M-1}}\right]^T \\ \{q_e\} &= \left[\frac{\partial E_1^A}{\partial \boldsymbol{n}_1}\frac{\partial E_2^A}{\partial \boldsymbol{n}_2}\cdots\frac{\partial E_M^A}{\partial \boldsymbol{n}_M}\right]^T \\ \{\phi_h\} &= \left[H_z^A(0)\frac{\partial H_1^A}{\partial \boldsymbol{t}_1}\frac{\partial H_2^A}{\partial \boldsymbol{t}_2}\cdots\frac{\partial H_{M-1}^A}{\partial \boldsymbol{t}_{M-1}}\right]^T \\ \{q_h\} &= \left[\frac{\partial H_1^A}{\partial \boldsymbol{n}_1}\frac{\partial H_2^A}{\partial \boldsymbol{n}_2}\cdots\frac{\partial H_M^A}{\partial \boldsymbol{n}_M}\right]^T. \end{aligned}$$

Incorporation of the new unknowns entails the following continuity conditions along the interface boundary:

$$E_z^A(0) = E_z^B(0), \quad H_z^A(0) = H_z^B(0),$$
$$\frac{\partial E_z^A}{\partial t} = -\frac{\partial E_z^B}{\partial t}, \quad \frac{\partial H_z^A}{\partial t} = -\frac{\partial H_z^B}{\partial t}. \tag{38}$$

Making use of (36)–(38) and following the same way adopted to obtain (35), the final system of matrix equation is derived as

$$\begin{bmatrix} [K^A] & -[G^A] & [0] & [0] \\ [K^B] & \alpha_1[G^B] & -\frac{Z_0}{\varepsilon_{rB}}[D^B] & [0] \\ [0] & [0] & [K^A] & -[G^A] \\ \frac{1}{Z_0}[D^B] & [0] & [K^B] & \alpha_2[G^B] \end{bmatrix} \begin{bmatrix} \{\phi_e\} \\ \{q_e\} \\ \{\phi_h\} \\ \{q_h\} \end{bmatrix} = \begin{bmatrix} \{0\} \\ \{0\} \\ \{0\} \\ \{0\} \end{bmatrix}. \tag{39}$$

In (39), the matrices $[K^i]$ and $[G^i]$ $(i = A, B)$ are the same, respectively, as given by the ones in (10), only that the components of $[K^B]$ are now arranged as

$$[K^B] = \begin{bmatrix} K_{11} & -K_{12} & \cdots & -K_{1M} \\ K_{21} & -K_{22} & \cdots & -K_{2M} \\ \vdots & \vdots & \vdots & \vdots \\ K_{M1} & -K_{M2} & \cdots & -K_{MM} \end{bmatrix}$$

and $[L^i]$ no longer remains a diagonal matrix, but takes the form of the $[L^i]$ matrix shown at the bottom of the page. And finally, $[D^B]$ is given by the second matrix at the bottom of the page.

### B. Applications

*1) Circular Step-Index Fibers:* The structure of the axially symmetrical circular step- index fiber is shown in Fig. 10. For symmetry, one quarter of the structure is taken for simulation by the method described in subsection A. Fig. 11 shows the division of boundary of the quarter of the circular cross section into ten constant elements and the allocation of the same number of simulated charges. Note that the simulated charges are allocated individually for both the exterior and the interior domain on outside of the respective domain. The computation is carried out by assigning values of $\beta$ for a certain range of interest and solving (39) by determinant search technique. The dispersion curves obtained for the dominant and the next higher modes are shown in Fig. 12. A good degree of accuracy of the solutions are reflected from the comparison of the computed solutions with the exact ones [16]. Comparison is shown only for the dominant mode since this is the only mode for which exact solutions are available so far. Field distributions for the two modes are shown in Figs. 13 and 14, respectively. In order to have an idea about the computational measure of (39), it might as well be worth mentioning here about the CPU time taken by it. For example, to solve (39) by determinant search technique for a matrix size of 40 × 40, the CPU time taken is 0.76 sec. The computations are obtained on a Dynus GAIA 275 AXP personal super computer (CPU: 275 MHz DEC 21 064A).

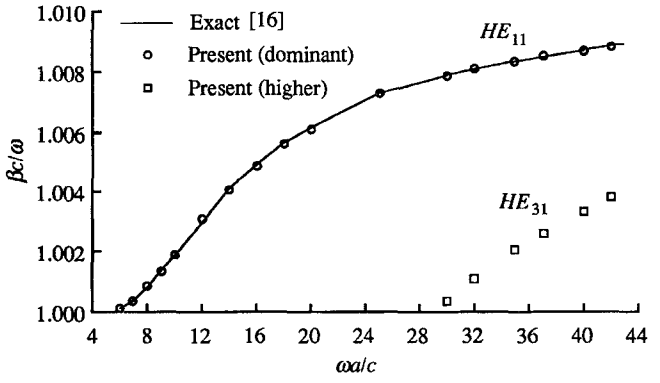


Fig. 12. Dispersion curve for dominant and higher modes for a circular step-index fiber.

*2) Rectangular Dielectric Waveguide:* Next, employing the same method as described in the previous subsection,

$$[L^i] = \begin{bmatrix} l_1 & \frac{l_1^2}{2} & 0 & 0 & \cdots & \cdots & \cdots \\ l_2 & l_1 l_2 & \frac{l_2^2}{2} & 0 & \cdots & \cdots & \cdots \\ \vdots & \vdots & \vdots & \vdots & \vdots & 0 & 0 \\ l_{M-1} & l_1 l_{M-1} & l_2 l_{M-1} & \cdots & \cdots & l_{M-2} l_{M-1} & \frac{l_{M-1}^2}{2} \\ l_M & \frac{l_1 l_M}{2} & \frac{l_2 l_M}{2} & \cdots & \cdots & \frac{l_{M-2} l_M}{2} & \frac{l_{M-1} l_M}{2} \end{bmatrix}$$

$$[D^B] = \begin{bmatrix} 0 & G_{11}^B - \frac{G_{1M}^B l_1}{l_M} & G_{12}^B - \frac{G_{1M}^B l_2}{l_M} & \cdots & G_{1M-1}^B - \frac{G_{1M}^B l_{M-1}}{l_M} \\ 0 & G_{21}^B - \frac{G_{2M}^B l_1}{l_M} & G_{22}^B - \frac{G_{2M}^B l_2}{l_M} & \cdots & G_{2M-1}^B - \frac{G_{2M}^B l_{M-1}}{l_M} \\ \vdots & \vdots & \vdots & \cdots & \vdots \\ 0 & G_{M1}^B - \frac{G_{MM}^B l_1}{l_M} & G_{M2}^B - \frac{G_{MM}^B l_2}{l_M} & \cdots & G_{MM-1}^B - \frac{G_{MM}^B l_{M-1}}{l_M} \end{bmatrix}$$

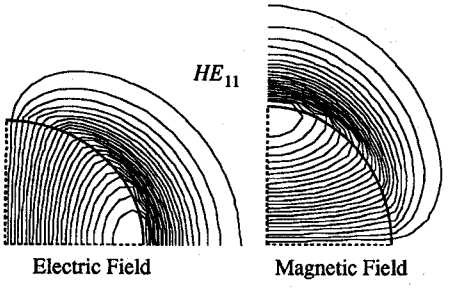


Fig. 13. Field distributions for the $HE_{11}$ mode.

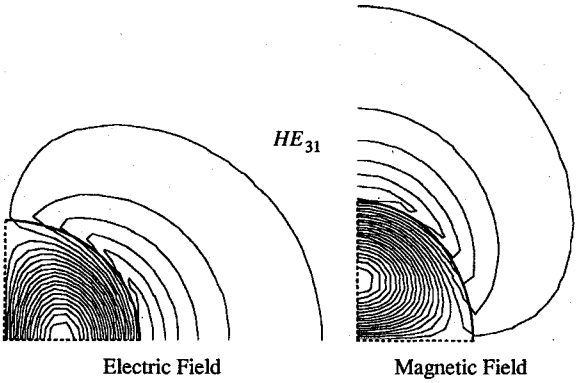


Fig. 14. Field distributions for the $HE_{31}$ mode.

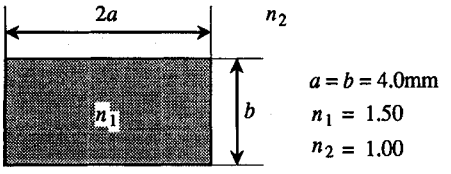


Fig. 15. Rectangular dielectric waveguide.

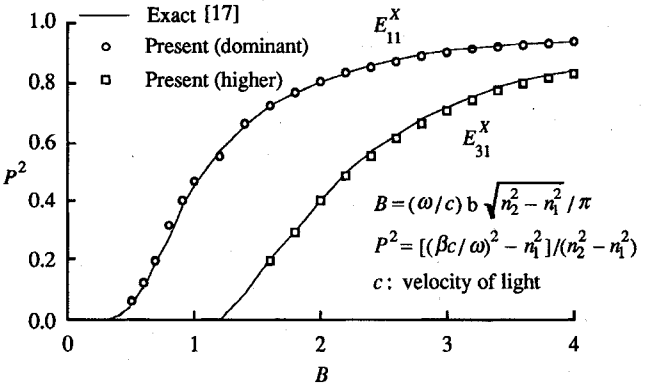


Fig. 16. Dispersion curve for dominant and higher modes for a rectangular dielectric waveguide.

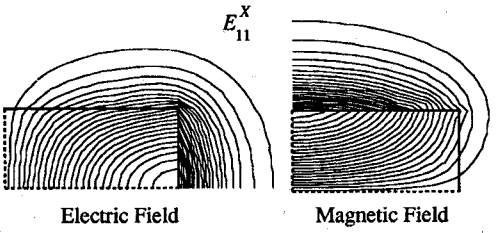


Fig. 17. Field distributions for the $E_{11}^x$ mode.

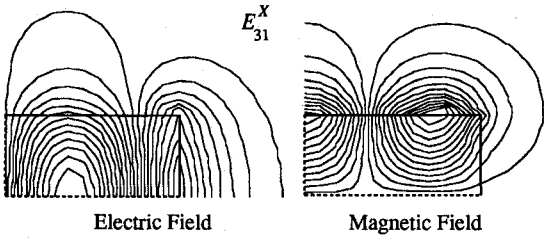


Fig. 18. Field distributions for the $E_{31}^x$ mode.

simulation is carried out for the rectangular waveguide shown in Fig. 15. Again, for symmetry, one quarter of the rectangular structure is considered. As shown for the circular step-index fiber, here, in the same way, the quarter of the rectangular boundary is divided into 10 constant elements and the same number of simulated charges are allocated outside the domains along the boundary. Fig. 16 shows the dispersion curves obtained for the modes $E_{11}^x$ and $E_{31}^x$. For comparison, solutions obtained by Goel [17] are also shown which are found to be in well agreement with the ones obtained by the present method. Field distributions for the two modes are shown in Figs. 17 and 18, respectively.

## V. Conclusion

We have developed and demonstrated the variational expressions for the regular BEM in the waveguide analysis. Gradual developments of the formulations have been laid down showing its versatile application in the waveguiding problems starting from simple hollow waveguides dealing with transverse modes to dielectric and optical waveguides dealing with hybrid modes. As the singular points of the fundamental solutions are located outside the domain, the formulations are enriched with the merit of avoiding singular integrals. Moreover, the boundary element approach has facilitated the formulations rendering an easy application to unbounded structured problems. For the dielectric/optical waveguide analysis, the formulation is fixed to yield spurious-free solutions. What offsets the merits by a little is that as the parameter to be resolved spreads out in the discretized equation in a scattered manner, the formulations cannot be solved by standard eigenvalue solver but by determinant search technique.

## References

[1] S. Murashima, *Simulated Charge Method and its Applications.* Tokyo: Morikita Press, 1983.

[2] C. Patterson and M. A. Sheikh, "A regular boundary integral equations for fluid flow," *Int. J. Num. Meth. Fluids,* vol. 2, pp. 239–251, 1982.

[3] T. Honma, Y. Tanaka, and I. Kaji, "Three-dimensional analysis of convective diffusion equation using regular boundary element method," in *Proc. 2nd Symp. Boundary Element Method, JASCOME,* 1985, pp. 25–30.

[4] Y. Sun and Y. Kagawa, "Variational formulations for boundary elements—eigenvalue solutions in two-dimensional Helmholtz equations," *IEICE Trans.,* vol. 76-A, pp. 902–906, 1993, in Japanese.
[5] ——, "A variational approach to boundary elements—two-dimensional Laplace problem," *Int. J. Numerical Modeling: Electronic Networks, Devices Fields,* vol. 7, pp. 1–14, 1994.
[6] ——, "Regular boundary integral solution with dual and complementary variational formulations applied to two-dimensional Laplace problem," *Int. J. Numerical Modeling: Electronic Networks, Devices Fields,* vol. 8, pp. 127–137, 1995.
[7] H. Sano and S. Kurazono, "Analysis of dielectric waveguide problem by boundary element method," *IEICE Trans.,* vol. 68-B, pp. 1419–1427, 1985, in Japanese.
[8] P. Tong and J. N. Rossettos, *Finite-Element Method.* London: MIT Press, 1982.
[9] Y. Kagawa, *Finite and Boundary Element Methods for Electrical and Electronic Engineering.* Tokyo: Ohm-sha, 1984.
[10] M. Washizu and Y. Tanabe, "Formulation of electromagnetic wave analysis by boundary element method and its application to the analysis of RF cavities," *Trans. Inst. Elec. Eng. Japan,* vol. 106, 61-A 27, pp. 210–216, 1986, in Japanese.
[11] E. Andoh and N. Kamiya, "Eigenvalue analysis of Helmholtz equation by boundary element method," JSME, vol. 57C-543, pp. 3457–3462, 1991, in Japanese.
[12] P. W. Partridge and C. A. Brebbia, "The dual reciprocity boundary element method for the Helmholtz equation," *Proc. Int. Boundary Element Symp.* C. A. Brebbia and A. Chaudouet-Miranda, Eds., Computational mechanics publication and Springer-Verlag, 1990, pp. 543–555.
[13] R. E. Collin, *Field Theory of Guided Waves.* New York: McGraw-Hill, 1960.
[14] W. Schlosser and H. G. Unger, *Advances in Microwaves,* vol. 1. New York: Academic Press, 1966.
[15] P. B. John, "The solution of inhomogeneous waveguide problems using a transmission line matrix," *IEEE Trans. Microwave Theory Tech.* vol. MTT-22, pp. 209–215, 1974.
[16] J. Carson, S. P. Mead, and S. A. Schelkunoff, *Bell Sys. Tech. J.,* vol. 15, pp. 310, 1936.
[17] J. E. Goel, "A circular harmonic computer analysis of rectangular dielectric waveguides," *Bell Sys. Tech. J.*, vol. 48, pp. 2133–2160, 1969.

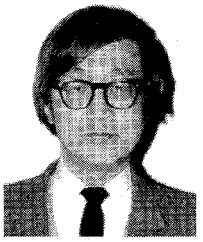

**Yukio Kagawa** (SM'75–F'86) received the B.Eng., M.Eng., and D.Eng. degrees in 1958, 1960, and 1963, respectively, all from Tohoku University, Japan.

In 1970, he was appointed Professor of Electrical Engineering Department, Toyama University, Japan. At present, he is a Professor of Electrical and Electronic Engineering Department, Okayama University and Professor Emeritus of Toyama University. His current research interests include application of the numerical approach to the simulation of acoustic and electromagnetic field system, in particular, inverse problems.

Dr. Kagawa is a Fellow of Institute of Acoustics (U.K.) and Vice President of the Japan Society of Simulation Technology.

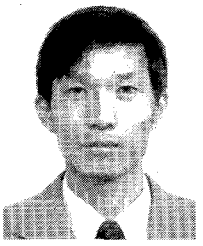

**Yonghao Sun** received the B.Eng. and M.Eng. degrees from Heilongjian University of China, in 1982 and 1987, respectively. He received the Ph.D. degree in electronics for intelligence from Okayama University, Japan, in 1996.

He is currently an Instructor in the Department of Electrical and Electronic Engineering of the same University. His research interests include numerical analysis of electromagnetic fields.

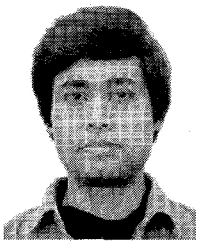

**Zaheed Mahmood** received the B.Sc. degree in electrical and electronic engineering from Bangladesh University of Engineering and Technology (BUET), Dhaka, in 1986. He received the M.Eng. degree in electrical and electronic engineering from Toyama University, Japan, in 1992 and the Ph.D degree in electronics for intelligence from Okayama University, Japan, in 1996.

He has been engaged in research on microwave field theory, and development and application of numerical methods to field problems.